Effect of degassing on scaling in hypersaline system: Tuzla geothermal field, Turkey

Serhat Tonkul, Laurent André, Alper Baba, Mustafa M Demir, Simona Regenspurg, Katrin Kieling

Tonkul *et al. Geothermal Energy* (2025) 13:5
https://doi.org/10.1186/s40517-024-00320-7

Geothermal Energy

RESEARCH Open Access

Effect of degassing on scaling in hypersaline system: Tuzla geothermal field, Turkey

Serhat Tonkul[1,7*], Laurent André[2,6], Alper Baba[3], Mustafa M. Demir[4], Simona Regenspurg[5] and Katrin Kieling[5]

*Correspondence:
s.tonkul-1@tudelft.nl

[1] Department of Environmental Engineering, İzmir Institute of Technology, Gülbahçe, 35430 Urla, İzmir, Turkey
[2] BRGM, 45060 Orléans, France
[3] Department of International Water Resources, İzmir Institute of Technology, Gülbahçe, 35430 Urla, İzmir, Turkey
[4] Department of Material Science and Engineering, İzmir Institute of Technology, Gülbahçe, 35430 Urla, İzmir, Turkey
[5] Helmholtz-Zentrum Potsdam, Deutsches GeoForschungsZentrum GFZ, Potsdam, Germany
[6] ISTO, UMR 7327, Univ Orleans, CNRS, BRGM, OSUC, 45071 Orléans, France
[7] Faculty of Civil Engineering and Geosciences, Delft University of Technology, Delft, The Netherlands

Abstract

A serious issue with geothermal power plants is the loss of production and decline in power plant efficiency. Scaling, also known as mineral precipitation, is one of the frequently-observed issue that causes this loss and decreasing efficiency. It is heavily observed in the production wells when the geothermal fluid rises from the depths due to a change in the fluid's physical and chemical properties. Scaling issue in geothermal power plants result in significant output losses and lower plant effectiveness. In rare instances, it might even result in the power plant being shut down. The chemistry of the geothermal fluid, non-condensable gases, pH, temperature and pressure changes in the process from production to reinjection, power plant type and design, and sometimes the materials used can also play an active role in the scaling that will occur in a geothermal system. ICP–MS was used to evaluate the chemical properties of the fluids. On the other hand, XRD, XRF and SEM were used to investigate the chemical and mineralogical compositions of the scale samples in analytical methods. For the numerical approach, PhreeqC and GWELL codes were used to follow the chemical reactivity of the geothermal fluid in Tuzla production well. The novelty of this study is to determine potential degassing point and to characterize the mineralogical assemblage formed in the well because of the fluid composition, temperature and pressure variations. During production, geothermal fluids degas in the wellbore. This causes a drastic modification of the chemistry of the Tuzla fluids. This is why it is focused the calculations on the nature of the minerals that are able to precipitate inside the well. According to simulation results, the degassing point is estimated to be about 105 m depth, consistent with the field observations. If a small quantity of precipitated minerals is predicted before the boiling point, degassing significantly changes the fluid chemistry, and the model predicts the deposition of calcite along with smaller elements including galena, barite, and quartz. The simulation results are consistent with the mineral composition of scaling collected in the well.

Keywords: Geothermal energy, CO_2 degassing, Scales characterizations, Geochemical modelling

Introduction

One of the main problems related to the extraction and utilisation of geothermal fluids is scaling. Especially, in high-temperature liquid-dominated geothermal systems, during the operation of wells, differences in temperature and pressure lead to changes in the chemical composition of the geothermal fluid and this causes calcification

problems. It is well known that the chemical composition of geothermal fluid in deep reservoirs is controlled by lithology. In particular, the interaction between the fluid and rocks leads to the dissolution of various minerals at different temperatures and pressures and mineral enrichment of the fluid. (Gunnlaugsson and Einarsson 1989; Kristmannsdóttir 1989; Honegger et al. 1989; Ölçenoğlu 1986; Pátzay et al. 2003). The chemical composition of a geothermal fluid is influenced by the temperature and pressure while being extracted from a reservoir. As a result, the pH and CO_2 content of the fluid create different types of scale problems in the well and surface equipment (Garcia et al. 2005). The scale issue arises from the supersaturation of dissolved minerals in the geothermal fluid, which is regulated by all of these variables. In geothermal wells, scaling restricts the flow of geothermal fluid, lowers system efficiency, and raises maintenance expenses. For example, Turkish geothermal fluids reduce production loss by 50% and generate scale difficulties in power plants with a thickness of approximately 3 cm (Tut-Haklıdır and Özen-Balaban 2019, Ölçenoğlu 1986; Şimşek et al. 2005).

In geothermal power plants, the most prevalent scale types are sulfide-type (particularly stibnite), carbonates (mainly calcite), and silica (Arnórsson 1989; Juranek et al. 1987; Potapov et al. 2001). Geothermal fluids from geothermal wells with silica and calcite deposits are typically also enriched in minerals such as iron magnesium silicate, magnesium silicate, calcium sulphate, and aluminum silicate; on the other hand, geothermal fluids from power plants with stibnite deposits are typically enriched in sulphide and sulfosalt minerals (Gunnlaugsson and Einarsson 1989; Honegger et al. 1989; Kristmannsdottir 1989; Ölçenoğlu 1986; Pátzay et al. 2003). Theoretical research on calcite scaling by Arnórsson (1989) revealed a boiling-related drop in CO_2 partial pressure. According to Arnórsson (1989), abundant of $CaCO_3$ in geothermal power plants stems from its deposition from extensively boiling ascending water. The researcher stated that calcite precipitates and supersaturates when CO_2 partial pressures drop sharply during boiling, and shortly after the boiling process begins, the supersaturation reaches its maximum. This provided evidence in favor of calcite scaling and supersaturation.

In the initial stage of boiling in a geothermal well, calcite scaling occurs, and during wastewater discharge, silica scale follows. Accordingly, calcite occurs in production wells, separator systems, and pipe/transmission lines, sulfide occurs in condensers, cooling towers, and heat exchangers, and silica-based scaling takes place in heat exchangers and reinjection wells (Pátzay et al. 2003). There may be a problem with silica scaling in geothermal fields with medium and high enthalpies. Different kinds of silica minerals can be found in hydrothermal zones at different depths. The most popular ones include quartz, cristobalite, chalcedony, and amorphous silica (Brown 2011). The most stable silica is quartz, which is the least soluble of these silica varieties. The solubility of amorphous silica in geothermal fluids declines with temperature in equipment where steam separation and cooling occur, which is problematic. Therefore, in geothermal power plants, transmission lines, heat exchangers, reinjection wells, and occasionally production wells are the riskiest equipment for amorphous silica scaling (Utami 2000; Demir et al. 2014; Mundhenk et al. 2013; Gunnarsson and Arnórsson 2005; Pambudi et al. 2015; Baba et al. 2015).

As shown in Fig. 1, the solubility of different forms of silica in water decreases as the temperature decreases. Based on Fig. 1, thermodynamically, amorphous silica will precipitate in priority with respect to other silica forms (Fournier and Truesdell 1973).

The whole nature of silica scaling is yet unknown, because it is more intricate than other types. For example, the kinetics of the silicic acid ($Si(OH)_4$) polymerization control silica scaling, in contrast to calcite scaling (Ellis and Mahon 1977). Equations 1 and 2 express this silica polymerization:

$$Si(OH)_4 \rightarrow (HO_3)SiOSi(OH)_3 + H_2O \tag{1}$$

$$OFeOH \cdot H_2O + 2Si(OH)_4 \rightarrow OFeOSi(OH)_3 + 2H_2O \tag{2}$$

The initial stage of silica polymerization is defined by these 2 processes. Amorphous silica is found in some geothermal fields in combination with Al^{2+} and Fe^{2+} to generate metal silicates (Gallup 1997). One of these metal silicates is represented by the Fe–O–Si bonds in Eq. 2. The Al–O–Si group is another group of metal silicates. The presence of Al ions and Fe ions in geothermal fluids causes amorphous silica scale (Brown 2011). While the concentration of Al ion in geothermal fluids seldom rises over 5 mg/l, 10% of the weight of the fluid is contributed by this value to the production of scale (Al_2O_3–SiO_2) (Ichikuni 1983; Gallup 1997; Yokoyama et al. 2002; Usda et al. 2003; Ikeda and Ueda 2017).

Compared to other forms of scale, silica deposits present the most difficulties in scale removal due to their complexity. This is a result of silica deposits' resistance to mechanical cleaning and inertness to a wide range of solvents. The solution approaches to avoid and reduce silica scaling involved examining the efficacy of using organic inhibitors and adjusting pH (Baba et al. 2015; Gallup 2002; Gallup and Barcelon 2005). The literature includes a number of studies on scaling.

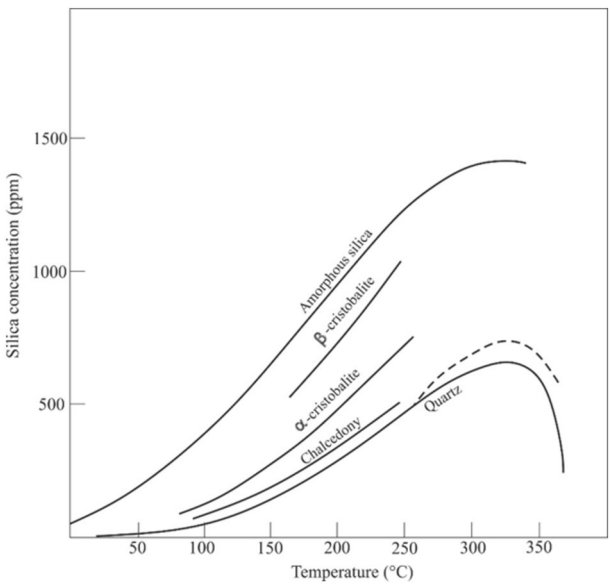

Fig. 1 Solubility of different silica forms in water (Fournier and Truesdell 1973)

Using data from new wells and the installation of two new power plants in the Kızıldere geothermal field, Tut-Haklıdır et al. (2021) assessed the reservoir characteristics of the field. The authors handled the mineral precipitation problem in the triple flash system. They used the test equipment system, such as a silencer, weir-box system, and separator, to collect fluid samples under changeable production settings that were managed by physical characteristics including temperature, pressure, and well flow rate. Their analyses revealed that when the reservoir temperature rises, there are more intense interactions between the water and rock. The authors stated that calcite and silicate scales are the most common scale types of Kızıldere field. Their modeling results showed that Al-silicates and Mg-silicates are significant scale types in the shallow wells. Using the ECO2N equation of state module in TOUGHREACT software, the flash point and scaling sites of two geothermal wells are numerically simulated by Cao et al. (2024). Their study is conducted to examine the variables influencing the flash point and scaling locations of geothermal wells. In addition, the impact of wellbore diameter, CO_2 mass flow rate, and liquid mass flow rate on the sites of flash point and calcite scaling are examined. TOUGHREACT established the T–H–C coupling method of geothermal fluid flow process from wellhead to well bottom. According to their simulations, the concentrations of Ca^{2+}, Cl^{-}, and Na^{+} in the geothermal fluid remain the same below the flash point. The results of TOUGHREACT simulations indicate that the concentration of Ca^{2+} drops quickly at the flash point and then gradually increases, whereas the concentrations of Cl^{-} and Na^{+} continuously increase. The amount of calcite scaling is lower below the flash point and increases significantly following flashing. Moreover, as the liquid mass flow rate, wellbore diameter, and CO_2 mass flow rate increase, the locations of the flash point and calcite scaling become deeper. Cao et al. (2024) concluded that the TOUGHREACT software-based THC model has demonstrated its ability to precisely forecast the scaling location of geothermal wells when compared to data observed on-site. Furthermore, when compared to current logging techniques like caliper logging equipment and sinker bar (go-devil), they concluded that the numerical simulation method is far more affordable when it comes to human, material, and financial resources.

Tobler and Benning (2013) aimed to measure the kinetics and mechanisms of silica nanoparticle nucleation and growth in conditions that largely resemble geothermal system. A synchrotron-based small angle X-ray scattering (SAXS) and a conventional dynamic light scattering (DLS) detector were used in experiments. Experiments were carried out using a flow geothermal simulator system in the study, where a real-time, in situ method was used in which a hot, supersaturated silica solution at 230 °C was rapidly cooled to initiate silica polymerization. With the help of this geothermal simulator, it was possible to monitor the initial stages of polymerization in real-time as well as the subsequent nucleation and development of silica nanoparticles in a cooling solution. The kinetic reactions were monitored, taking into account silica concentrations, ionic strengths, temperature, and pH. The results showed that the silica nanoparticle formation rate was proportional to the silica concentration (640 vs. 960 ppm SiO_2), and the first detected particles were spheres with a diameter of approximately 3 nm. Tobler and Benning (2013) concluded that the geothermal simulator system aligned with time resolved aqueous analyses and in situ and time-resolved particle formation. Andhika et al. (2015) studied the polymerization of silica and its precipitation using geochemical

and mineralogical methods. The relationship between precipitation reactions and temperature, pH, and ionic strength were studied. Silica polymerizations were monitored using ultrasonic measurements (e.g. ultrasonic velocity) based on the change in compressibility, temperature, and density of a solution. Andhika et al. (2015) mentioned that since compressibility at constant temperature and density is inversely proportional to ion concentration, changes in silica concentration can be detected by measuring ultrasonic velocity, providing insight into the polymerization and precipitation processes. Ultrasonic velocity in 500 ppm silica solutions was measured at different pH values, and it was concluded that the ultrasonic velocity dropped as the pH declined, possibly indicating silica polymerization.

Kristmannsdóttir (1989) stated that the most important use of geothermal energy in Iceland is for space heating and mentioned a typical issue with reinjection wells is iron–magnesium silicates in the Reykjanes field. Along with silica scaling, sulfide deposits are precipitated in the surface equipment system of the Reykjanes field. Semi-quantitative analyses showed that the scale samples are mostly composed of Fe, Zn, and Cu sulfides with some silica and traces of Ca and K. Although the composition of the weakly crystalline scales varies, they resemble some of the precipitates detected in the altered rocks throughout the well drilling process. On the other hand, Kristmannsdóttir (1989) explained that many fluids with low temperatures include some hydrogen sulfide, which can coat steel pipes in iron sulfide and effectively erode copper surfaces, especially in Northern Iceland.

Köhl et al. (2020) pointed out thermodynamic models based on equilibrium overestimate the scaling potential and have used regression functions to measure the impact of various scaling factors. The linear regressions that are employed to predict the scale rate at the wellhead and across the production pipe are made possible by the correlations. The authors used two different approaches to evaluate carbonate scale rates. The first approach explains using of hydrogeochemical models. The second approach relies on correlations between thermodynamic scale drivers (total pressure, pH, saturation indices for calcite) and measured wellhead scale rates at six different facilities. According to the modeling results, scale prediction based on the new regressions that depend on thermodynamic scale drivers performed better than hydrogeochemical models that are already in use without kinetic parameter implementation. Akhmedov (2009) created a kinetic model to determine the rate at which calcium carbonate is formed. The author evaluated the growth rates of suspended solids, which are composed of calcium carbonate crystals in geothermal fluids. Transfer of suspended particles was described by particle motion inertia and turbulent pulsations, and Akhmedov (2009) concluded that suspended particles play an important role in the formation of calcium carbonate deposits. Ryley (1980) investigated the correlation between mass discharge and wellhead pressure in a geothermal well using reservoir lithology and frictional losses as model. The model evaluated the various effects of reservoir drawdown, variation in the friction factor, and the degree of phase slip in the exit section parametrically by considering inlet and outlet pressure of the wellbore. To comprehend the impacts of heat exchange with altitude, non-condensable gases (NCGs), and salts in geothermal wells, Barelli et al. (1982) concentrated on a two-phase flow model that describes the impacts of the presence of salts on noncondensable gases (NCGs) using thermodynamic parameters, including enthalpy, density, and

brine vapour pressure. Barelli et al. (1982) compared the numerical and experimental results and concluded that the NCGs were significant for these computations, even at very low concentrations.

A mathematical model for predicting calcite formation rates and analyzing how calcite formation affects flow rates was studied by Satman et al. (1999). The authors used an analytical model to evaluate reservoir and operating conditions. According to their analytical model, the degree of calcite deposition or clogging surrounding the well can be significantly decreased for a given brine flow rate by either reducing the pressure gradient close to the well or by increasing the effective wellbore radius using well-stimulation procedures. On the other hand, Cerclet et al. (2023) aimed to quantify the parameters impacting the calcite scaling by calibrating a thermo-hydro-chemical model using experimental data. They used 16 groundwater samples to calibrate a thermo-hydro-chemical model which includes CO_2 degassing, calcite reactions, and temperature dependent reactions. Cerclet et al. (2023) stated that the degassing of CO_2 causes a 36% increase in calcite precipitation, primarily at high temperatures, according to their numerical results.

As can be seen, reduced fluid flow, as induced by scaling or degassing, is one of the largest obstacles for safe, reliable, economic, and long-term geothermal operations. The prevention of obstructions to flow, caused by either solids or gases, in a geothermal loop, is important to understand, and it requires the exact degas point to be known.

The main problem in the Tuzla Geothermal Field (TGF) is silica-based scale formation, carbonate deposits and the degassing has a significant impact on the Tuzla fluid chemistry. Although many studies have been carried out on scaling problems in the TGF so far, the geochemical properties and behaviour of the fluid have not been fully understood due to the complex nature of the region. This study is based both on field observations and modelling results. Indeed, geochemical calculations are used to characterize the chemical behaviour of the geothermal fluid in the well, i.e., between the reservoir and the wellhead. The numerical simulations follow the evolution of the chemical composition of the fluid according to temperature and pressure changes inside the well and they predict the nature of the minerals that are able to precipitate inside the well according to a semi-quantitative approach.

Geology of the Tuzla geothermal system

Studies on geothermal energy were initiated in Türkiye throughout the 1960s. The General Directorate of Mineral Research and Exploration (MTA) conducted the initial research based on these studies and 170 geothermal areas with fluid temperatures higher than 40 °C were identified. Being an active fault zone and one of Turkey's most important geothermal sources, Tuzla and its environs have been the focus of several geological studies in the past (Ercan and Türkecan 1985; Karamanderesi 1986; Mützenberg 1990; Samilgil 1966; Şener and Gevrek 2000). The TGF is an active tectonic field situated 80 km south of Çanakkale and 5 km from the Aegean Sea, Türkiye (Fig. 2). The 50 km^2 region covered by the geothermal field includes the Tuzla River and its tributaries. Researches on geothermal energy have been continuing in the field since 1966. Many scientists have studied the fundamental geological features and volcanology of the region (Alpin 1976; Samilgil 1966; Urgun 1971). However, the physical

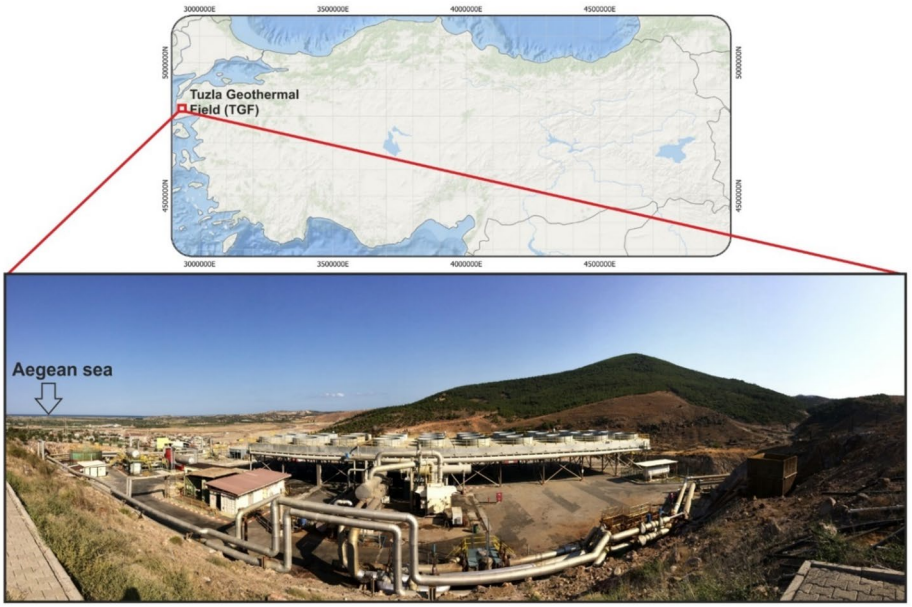

Fig. 2 Location map of the TGF

and chemical properties of the geothermal fluid in the region have yet to be understood due to its complex tectonic structure. For this reason, the 3D conceptual model of the TGF was created using the Leapfrog Geothermal software (© Seequent Limited). The present 3D conceptual model is made up of structural controls, geothermal wells, and lithological units (Figs. 3 and 4). The basement is composed of metamorphic rocks that are Paleozoic in age. Recrystallized Palaeozoic limestones with angular unconformity covers this basement. Rhyolitic tuffs, ignimbrites, latitic lavas, and rhyolitic lavas of Miocene age, which are the byproducts of calcic volcanism, make up the upper portion of the stratigraphic layer (Şener and Gevrek 2000). The reservoir rocks consist of these Miocene aged volcanic rocks. The cover rocks in the system are of Neogene sandstone and claystone origin. Sandstone, limestone, conglomerate and clayey limestone sediments form the upper Miocene to Pliocene sediments overlying ignimbrites formed during the last phase of volcanism in the region. The Tuzla Plain was deposited by the Quaternary alluvium, which is at the top of the stratigraphic layer. Following Miocene volcanism, the Tuzla geothermal fluid is a region linked to hydrothermal activity and characterizes the active thermal regime (Şener and Gevrek 2000). Volcanism is currently linked to the TGF's active thermal regime.

Materials and methods

The methods used in this study can be divided into analytical and numerical. The scale samples and fluid samples from geothermal wells were thus collected as part of the field research. The analytical methods aim to ascertain the primary anions and cations in fluid analysis, assess the quantities of heavy metals, and conduct XRD, XRF, and SEM analyses on scale samples.

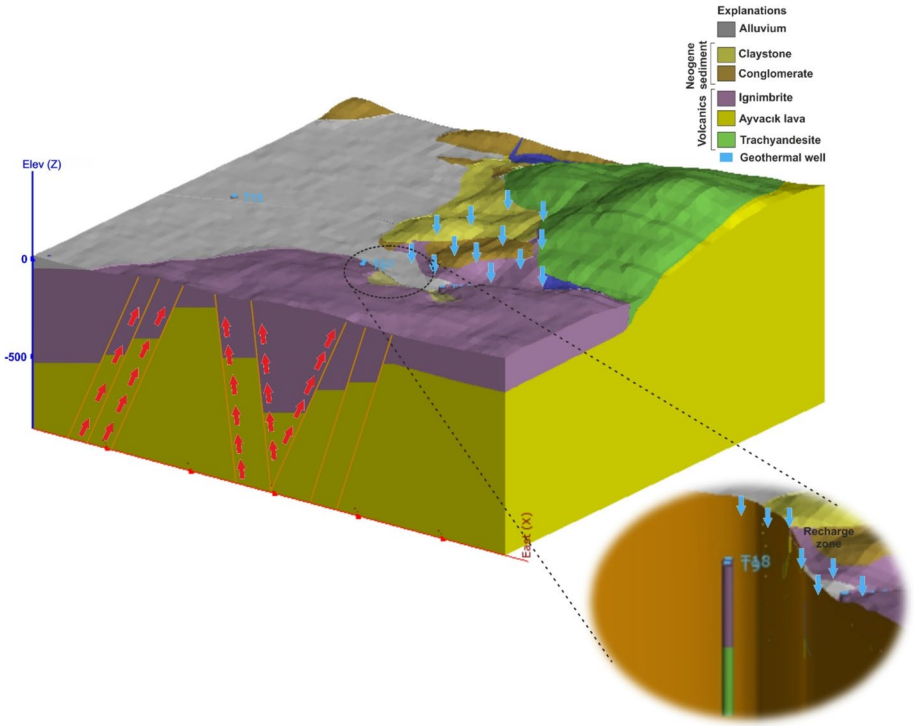

Fig. 3. 3D conceptual model of the Tuzla geothermal field

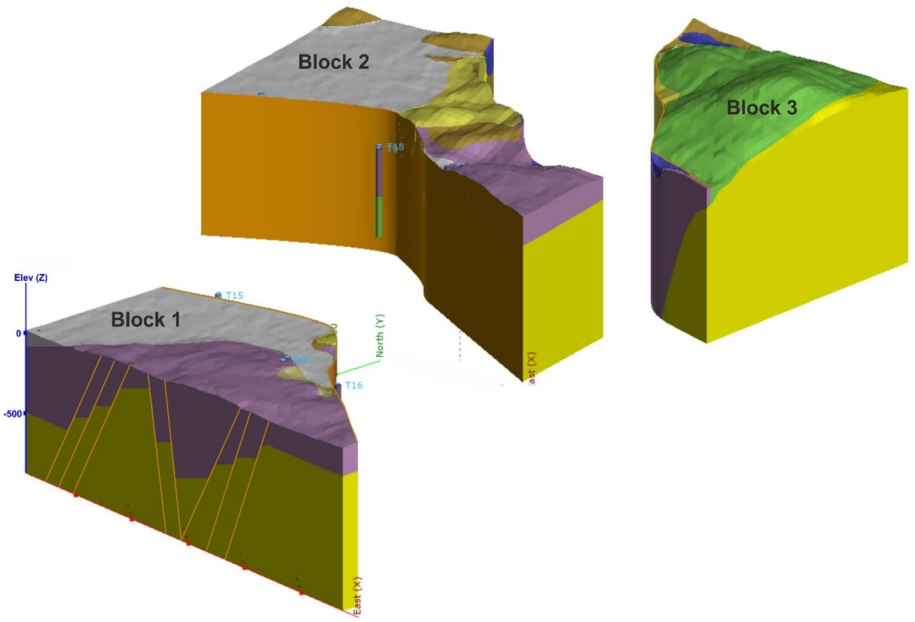

Fig. 4 Cross section of 3D conceptual model of the Tuzla geothermal field

For the numerical approach, PhreeqC-3 (Parkhurst and Appelo 2013) and GWELL (Aunzo et al. 1991) codes are used to follow the chemical reactivity of the geothermal fluid in the production well. Flow chart for the research methodology is given in Fig. 5.

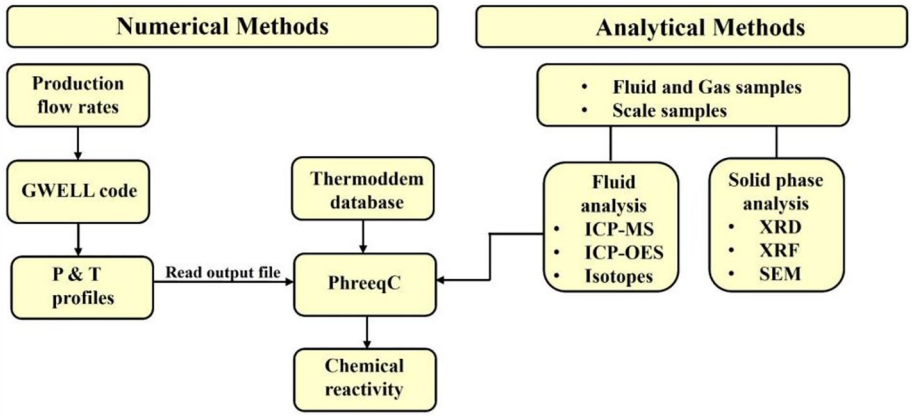

Fig. 5 Flow chart for the research methodology

Table 1 Well information from the TGF

Well ID	Well depth (m)	Bottom hole temperature (°C)	Wellhead temperature (°C)	Geothermal gradient in well (°C/m)	Flow rate (t/h)	Bottom pressure (bar)	Wellhead pressure (bar)
T9	540	174.04	164.47	2–3 °C/50 m	316	46.41	2.11
T15	871	–	105	–	–	–	–
T16	556.5	174.98	166.3	2–3 °C/50 m	275	47.4	2.42
T18	550	173	168.6	3–4 °C/50 m	300	43.59	2.14

Analytical methods

Geothermal fluid and gas samples

Geothermal fluid samples were collected from wells and surface equipment systems. Table 1 provides details about the well information in the TGF. Geothermal fluid samples were collected from the wellheads before to the separator in the study field. 100 ml HDPE bottles for heavy metal analysis, 250 ml for major–minor anions and cations, and 1 L for stable isotopes were utilized. Samples were collected for heavy metal analysis, and then 2% HNO_3 (nitric acid) was added to acidify them. In the laboratories of the Izmir Institute of Technology, major and minor studies were carried out using ICP–MS (Inductively Coupled Plasma Mass Spectrometry), while heavy metal analyses were carried out using ICP–OES (Inductively Coupled Plasma Optical Emission Spectroscopy) equipment. Through the use of the Hach-Lange DR5000 UV-spectrophotometric technique, the SiO_2 concentrations of the geothermal fluids were ascertained. In the laboratories of the State Hydraulic Works (DSİ) in Ankara, Türkiye, stable isotope analysis of the geothermal fluids was performed. An Omnistar (Pfeiffer Vacuum) quadrupole mass spectrometer with a closed ion source and a mass range of 1–100 amu was used in the GFZ laboratories (GFZ Helmholtz Centre, Potsdam) to analyze the chemical composition of gas samples (H_2, He, N_2, CH_4, Ar, and CO_2).

Analyzing the scale samples

The scale samples were collected from some of the geothermal wells and surface equipment. X-ray crystallography (XRD), X-ray fluorescence spectroscopy (XRF), and scanning electron microscope (SEM) analyses were performed on scale samples. Using the Spectro IQ II instrument, XRF studies of scale samples collected from geothermal wells were carried out. High sensitivity element concentration delivery at the ppm level is possible with Spectro IQ II, ranging from sodium (Na-11) to uranium (U-92). In addition, X-ray diffraction (XRD) studies of scale samples were carried out utilizing the Philips X'Pert Pro. X-ray diffraction (XRD) provides information on the material's crystal size, non-crystalline phase content, and phase concentration. The FEI QUANTA 250 FEG scanning electron microscope (SEM) was utilized to visualize the micro-sized scale formations.

Using numerical methods for understanding chemical reactivity

Understanding the mechanisms underlying depositional issues in production wells and surface facilities is made easier with the use of geochemical computations. They enable the type and quantity of precipitated minerals to be predicted. Thermoddem database (Blanc et al. 2012; https://thermoddem.brgm.fr/) and computational code PhreeqC-3 were utilized for this purpose, primarily to analyze the fluid's chemical reactivity.

PhreeqC is a code widely used in the geosciences community to deal with chemical reactivity of water with rocks and gases in different environments. This code allows in particular to take into account the effect of temperature on chemical equilibria by the dependence of the equilibrium constants K of each reaction according to the relationship $\mathrm{Log}_{10}\, K(T) = A + BT + C/T + D.\mathrm{Log}_{10}\, T + E/T^2 + F.T^2$, where *A, B, C, D, E, F* are coefficients entered in the thermodynamic database, in this case Thermoddem. The dependence on pressure, at a given temperature, is given as a first approximation by: $\mathrm{Log}_{10} K(T,P) = \log K(T,\ 1atm) - (P-1)/(RT.ln10)\ *\ \Delta V(T,P)$

ΔV(T,P) is in turn described by the HKF equation of state (Helgeson et al. 1981; Tanger and Helgeson 1988) for aqueous species. This term also assumes that the molar volume of the solids is constant. For the dissolution of gases, the equilibrium constant of the reaction is defined at 1 atm at any temperature, the effect of pressure being included in the calculation of the fugacity coefficient according to the Peng–Robinson equation.

The Tuzla geothermal fluids have high salinity; hence it makes more sense to have a database with a Pitzer formalism for saline waters. However, the redox conditions required to monitor, for instance, the reactivity of sulfate and sulfide minerals are not optimally present in this kind of database. We have selected a database like Thermoddem, which employs a B-dot activity model because of this. We have required the well's temperature and pressure conditions, because our goal was to monitor the chemical reactivity in the production well. For this reason, the P and T profiles in the wellbore were computed using the GWELL code.

PhreeqC and GWELL codes are used to follow the chemical reactivity of the geothermal fluid in the production well. For this, a three-step process is employed:

(i) Determination of the fluid's composition in the reservoir. Indeed, variations in temperature and pressure both during the upflow into the production well and during

sampling have an impact on the composition of the geothermalfluid. We need then to recalculate the fluid composition in the reservoir using the PhreeqC code under batch conditions. For that, we use the fluid composition that was analyzed at the surface (Table 2) and we impose to it some constraints given by reservoir conditions and described in "The Numerical Analysis Results" paragraph;

(ii) Determination of temperature and pressure profiles in the well. The GWELL code enables the calculation of P and T profiles in the well based on the well design (length, diameter, etc.) and the exploitation mass flows;

(iii) Determination of the chemical reactivity in the well. The PhreeqC code incorporates the temperature and pressure profiles that were computed using the GWELL code. A series of batch with their own couples (P, T) mimic a 1D well. Each batch is considered as a separate reactor with chemical reactions (equilibrium between the gaseous and aqueous phases and between the aqueous phase and the minerals) that occur within them. Initially, each batch is in equilibrium with a gas phase that has been initiated with zero composition and nil volume. As a result, the liquid can degas (that is, the gas phase can express) depending on the pressure and temperature. The input parameter is the chemical composition of the pumped liquid as described in step 1.

The calculations focus mainly on identifying the minerals that may precipitate inside the well as a function of temperature and pressure variations. All the geochemical calculations were carried out at equilibrium, between the gas phase, aqueous solutions and minerals. For this reason, the approach presented here is semi-quantitative, the main objective being to compare field observations with the results of the calculations. A full quantitative approach would require taking into account the kinetic precipitation rates of the minerals or a specific deposition model to simulate the evolution of the thickness of the deposits on the well walls. This objective is beyond the scope of this paper.

The results

Fluid and gas properties of the Tuzla geothermal fluids

The average pH and Electric Conductivity (EC) values in the TGF are, respectively, 5.6 to 7.65 and 83.2 to 90.0 mS/cm. Because of the high partial pressure of CO_2 gas in the well, there is an excess of free CO_2 (free mineral acidity) in the water from the wells, making the water acidic. At the Tuzla geothermal site, the wellhead temperatures of the geothermal fluid in wells T9, T16, and T18 are, respectively, 164.47 °C, 166.3 °C, and 168.6 °C. Na^+ and Cl^- are the predominant ions in the TGF geothermal fluid, based on the Piper and Schoeller diagrams (Figs. 6 and 7). Because of this high concentration of Na^+ and Cl^-, the geothermal fluid in the TGF is referred to as having a hyper-saline character. Hydrothermal activity is indicated by the TGF's geothermal fluids' high NaCl content, isotopic composition, and other characteristics. Geothermal fluids from depth are elevated by the region's active seismicity and hydrothermal activity. After cooling to a certain point, the upwelling geothermal fluid mixes with groundwater to become less concentrated (Baba and Tonkul 2022). When the pH change graphs in 2020 and 2021 are examined, there are significant

Table 2 Chemical composition of the geothermal brine produced from TGF

Well ID	T (°C)	pH	EC (µS/cm)	Ca^{2+} (ppm)	Mg^{2+} (ppm)	Na^{+} (ppm)	K^{+} (ppm)	Cl^{-} (ppm)	HCO_3^{-} (ppm)	SO_4^{2-} (ppm)	Si (ppm)	Sr (ppm)	Sb (ppm)
T9	160.8	5.6	85,340	2560	122	17,950	2210	34,840	135	227.4	176	130	0.06
T15	105	5.7	83,200	2850	114.5	16,800	1770	33,200	138.5	192.6	197	132.5	0.1
T16	166.3	5.8	83,990	2810	116	16,550	1745	31,350	180.6	180.6	196	131.5	0.02
T18	168.6	5.6	86,260	3020	111	17,700	1925	35,300	204	204	189	142.5	0.19

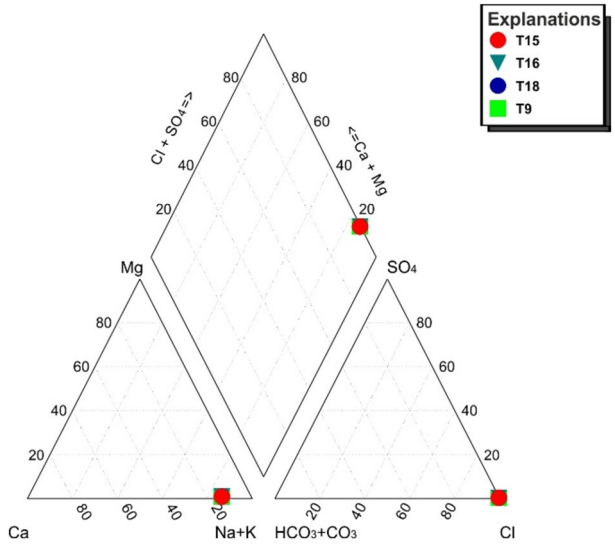

Fig. 6 Piper diagram of the geothermal fluids in the TGF

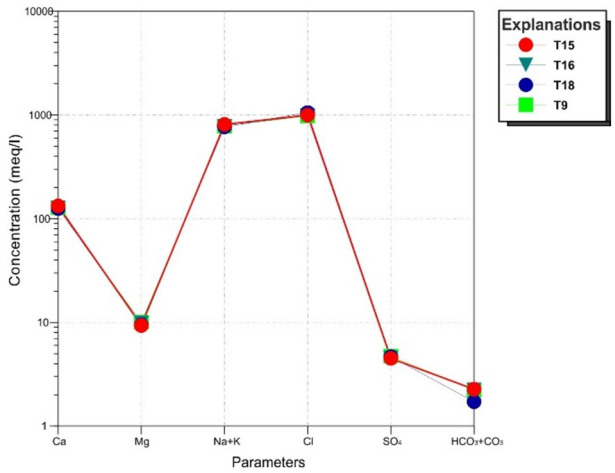

Fig. 7 Schoeller diagram of the geothermal fluids in the TGF

changes in the pH values before and after the separator. In both years, the pH values in the geothermal fluids collected before the separator (at wellhead) decreased. This is because the fluid is two-phase (gas + liquid) before the separator. CO_2, an acidic gas, decreases the pH values when present with liquid. On the other hand, an increase in the pH values is observed in the fluid samples collected after the separator due to the separation of gas and liquid (Figs. 8 and 9). In the EC graphs for 2020 and 2021, slight increases are observed in some months. The formation of Na-rich clays in the geothermal aquifer and the Ca/Na ion exchange caused by plagioclase albitization could be the reason for this (Kloppmann et al. 2001). In addition, Baba et al. (2009) stated that the interaction between fluid and volcanic rocks may affect the EC values. The EC values of the geothermal fluid don't change considerably in 2020 and 2021, and there are no significant fluctuations in the EC values

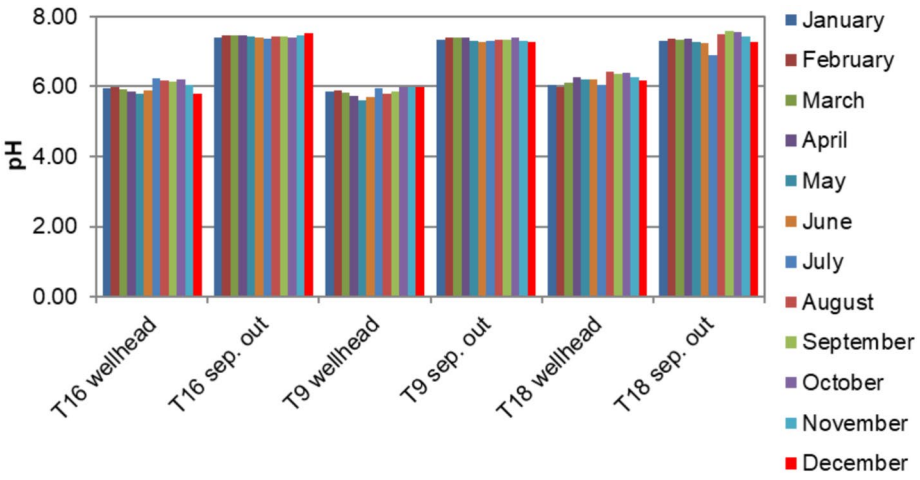

Fig. 8 pH change in the geothermal wells in 2020

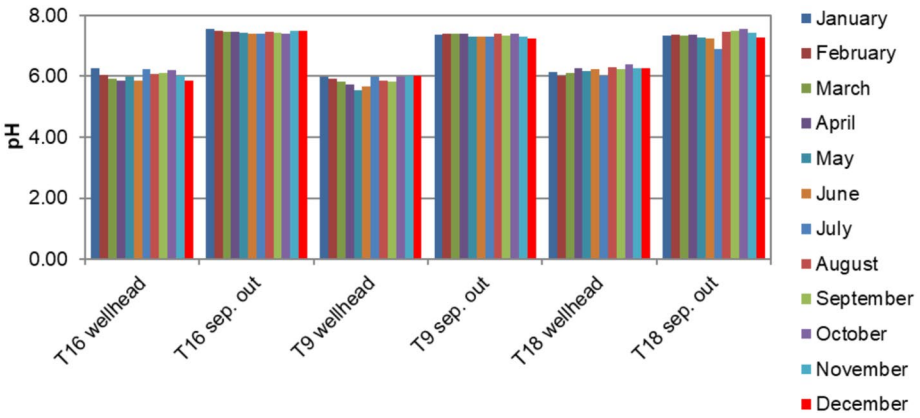

Fig. 9 pH change in the geothermal wells in 2021

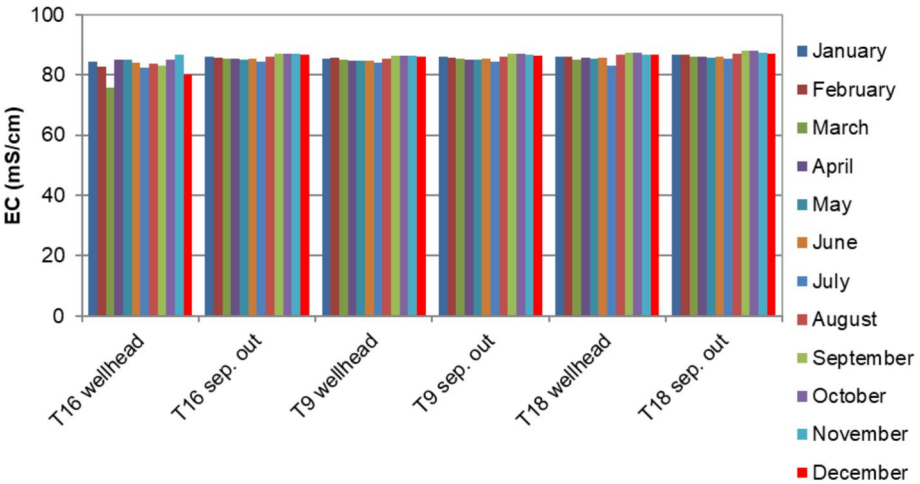

Fig. 10 EC change in the geothermal wells in 2020

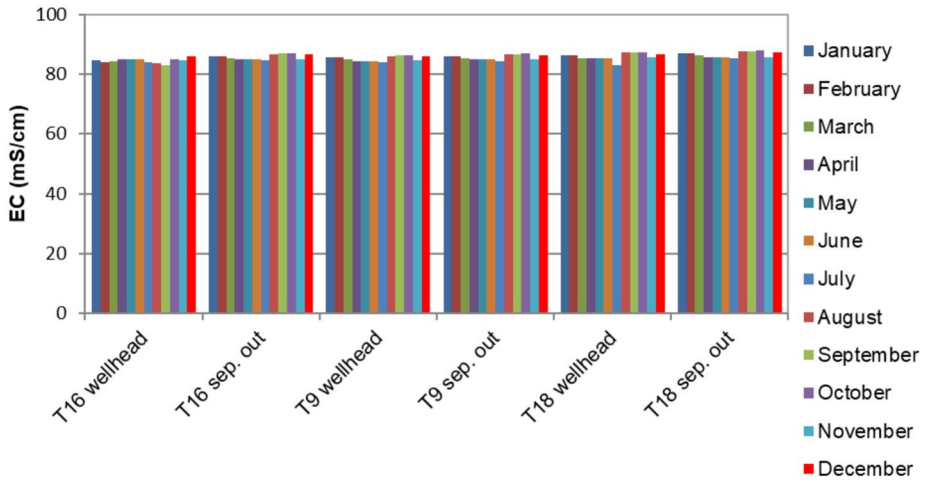

Fig. 11 EC change in the geothermal wells in 2021

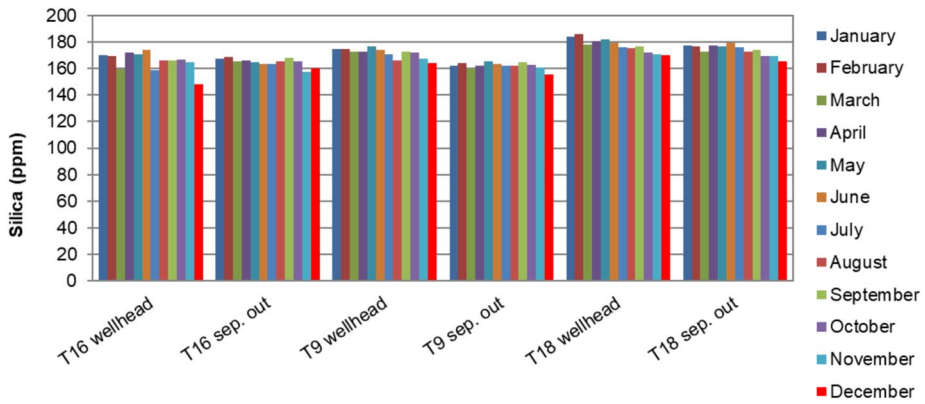

Fig. 12 Silica change in the geothermal wells in 2020

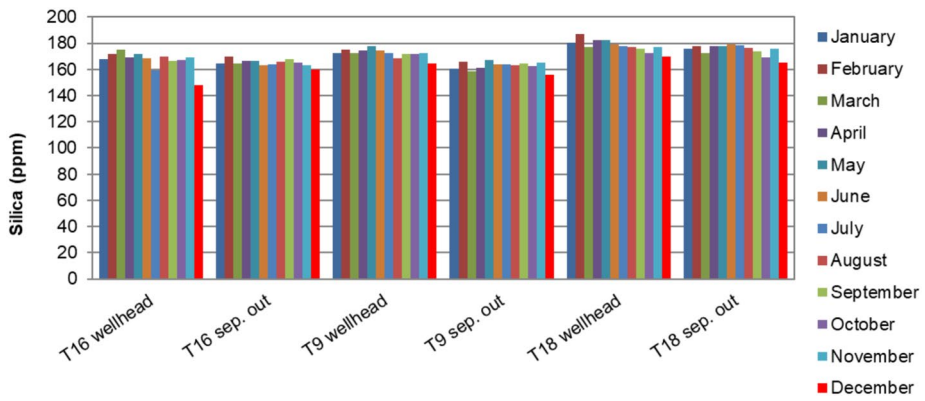

Fig. 13 Silica change in the geothermal wells in 2021

(Figs. 10 and 11). The small changes in silica values on a monthly basis are probably related to water circulation in the reservoir. When the silica values in 2020 and 2021 were compared, no significant change was observed. TGF has silica concentrations

Table 3 Gas composition of the Tuzla geothermal fluid

Vol. (%)	T9	T16	T18
Ar	0.177	0.081	0.063
CO_2	87.3	93.1	90.3
H_2	0.108	0.085	0.062
N_2	10.6	6.22	9.28
He	0.0144	0.0102	0.0102
CH_4	0.817	0.58	0.524

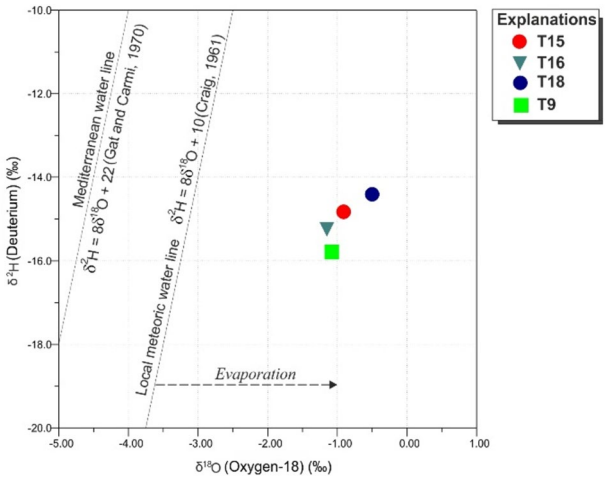

Fig. 14 Isotope evaluation of the Tuzla geothermal fluids

between 189 and 197 mg/l (Figs. 12 and 13). CO_2, ranging from 87.3 to 97.6% by volume, is the most dominant of all gases, followed by N_2, ranging from 1.55 to 10.6% by volume (Table 3). The Tuzla wells have the highest He contents, exceeding 100 vol. ppm. In well T9, the highest value of 144 vol. ppm was observed.

Stable isotope evaluation of the Tuzla geothermal fluids

Important details on the subterranean activities in geothermal reservoirs and the sources of thermal fluids can be evaluated with stable isotopes. Studies on the isotopes of hydrogen and oxygen were conducted to comprehend the development of geothermal fluids in the TGF. Standard Mean Ocean Water (SMOW) is used as a reference point when evaluating the isotopic composition of water. For all water isotope ratios published by Craig (1961), SMOW is regarded as the international standard Mediterranean water isotopes are provided by Gat and Charmi (1970). This indicates that in the geothermal fluids, the $\delta^{18}O$ isotope values range between − 0.5 and − 1.15, while the δD isotope values range between − 14.41 and − 15.79 (Fig. 14). Geothermal fluid has an enriched $\delta^{18}O$ concentration of up to − 0.5, while its depleted δD to − 15.79 indicates a large $\delta^{18}O$ shift caused by evaporation at higher

Table 4 Silica reservoir temperature equations used for the TGF

Geothermometer	Geothermometer equations	References
1	$T\,°C = -42.2 + 0.28832SiO_2$-3.6686 × 10–4 $SiO_2^2 + 3.1665 \times 10$-7S3 + 77.034log$SiO_2$	Fournier and Potter (1982)
2	$T\,°C = [1309/(5.19$-log$SiO_2)] - 273.15$	Fournier (1977)
3	$T\,°C = [1522/(5.75$-log$SiO_2)] - 273.15$	Fournier (1977)
4	$T\,°C = -55.3 + 0.36559SiO_2$-$5.3954 \times 10^{-4}SiO_2^2 + 5.5132 \times 10^{-7}SiO_2^3 + 74.360\log SiO_2$	Arnórsson (2000)
5	$T\,°C = [1032/(4.69$-log$SiO_2)] - 273.15$	Fournier (1977)
6	$T\,°C = (1112/(4.91$-log$SiO_2)) - 273.15$	Arnórsson et al. (1983)

Table 5 Na–K reservoir temperature equations used for the TGF

Geothermometer	Geothermometer equations	References
1	$T\,°C = 856/[\log(Na/K) + 0.857] - 273.15$	Truesdell (1976)
2	$T\,°C = 883/[\log(Na/K) + 0.780] - 273.15$	Tonani (1980)
3	$T\,°C = 933/[\log(Na/K) + 0.993] - 273.15$	Arnórsson et al. (1983)
4	$T\,°C = 1319/[\log(Na/K) + 1.699] - 273.15$	Arnórsson et al. (1983)
5	$T\,°C = 1217/[\log(Na/K) + 1.483] - 273.15$	Fournier and Potter (1979)
6	$T\,°C = 1178/[\log(Na/K) + 1.470] - 273.15$	Nieva and Nieva (1987)

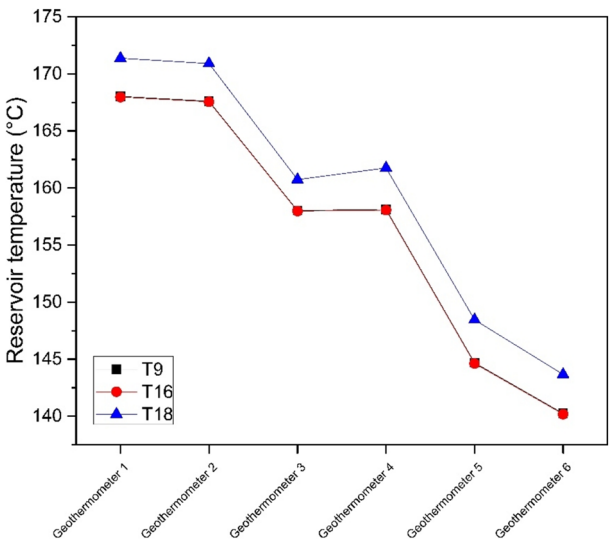

Fig. 15 Silica geothermometers

temperatures. The stable isotope data demonstrate that the TGF's geothermal fluids are derived from meteoric origin (Fig. 14).

Geothermometer applications

The reservoir temperatures of the Tuzla geothermal field were determined using cation and silica geothermometers. SiO_2 concentrations (as ppm) were derived from the chemical analysis results assessed in the TGF within the parameters of the study. The TGF has SiO_2 values ranging from 189 to 197 ppm. Tables 4 and 5 give the equations computed

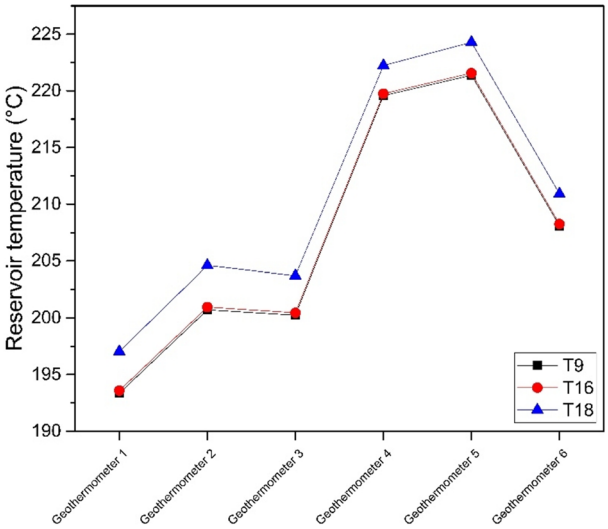

Fig. 16 Na–K geothermometers

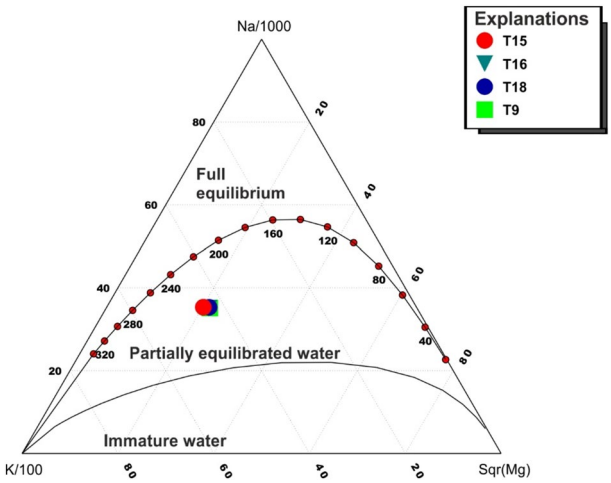

Fig. 17 Distribution of fluid samples from the TGF in a Na–K–Mg triangular diagram

using the silica and Na–K geothermometers for the geothermal fluids that constitute the geothermal aquifer. The temperatures of the reservoirs as determined using silica geothermometers range from 140 °C to 173 °C (Fig. 15). However, the reservoir temperature for the geothermal fluid in the TGF ranges from 193 °C to 222 °C, according to the Na/K geothermometer results (Fig. 16).

Giggenbach (1988) proposed the Na–K–Mg triangular diagram. A combination of Na/K and K–Mg geothermometers can be seen in the Giggenbach diagram. A helpful framework for understanding actual fluid and mineral compositions is the Giggenbach triangular diagram's zone of full equilibrium. It describes the entire iso-chemical re-crystallization of the main rock component at a specific temperature and pressure. The equilibrium line defines the immature and partially equilibrated water. It is also evident that there is a range in which the Na–K–Mg geothermometer can be

used reliably, from the disintegration of rocks to immature fluids. Approaching the geothermal fluids in the TGF to the Na^+ and K^+ line is related to the volcanic rocks, including andesite and trachyandesite units, as can be observed from the Giggenbach diagram (Fig. 17). The geothermal fluids in the TGF are only partially in equilibrium with the reservoir rocks, as can be shown in the Giggenbach triangular diagram (Fig. 17). As a result, the temperature of geothermal fluid samples cannot be applied using Na/K geothermometers, and Fig. 15 illustrates how the silica geothermometer's predicted temperatures appear to be more accurate.

In parallel to the use of several geothermometer equations to reconstruct the temperature distribution of the TGF, we also estimate the reservoir temperature by applying the PhreeqC code. It consists to start the calculation with the chemical composition of the geothermal fluid at lab conditions (i.e., 25 °C and 1 bar). And then, the temperature and pressure conditions are increased up to 200 °C and 50 bar (i.e., above the supposed reservoir conditions) and the evolution of saturation indices of many minerals (carbonates, silicates, sulfides and sulfates) are followed (Fig. 18). As expected, the saturation indices of silicates, sulfides and sulfates tend to decrease when temperature augments (prograde solubility), whereas the saturation indices of carbonates increases with temperature (retrograde solubility). By the end, all the saturation indices converge to a common equilibrium temperature, representative of reservoir temperature. Figure 19 confirms that the reservoir temperature is ranging between 160 and 170 °C.

Using wells with static temperature data, a reservoir temperature simulation was also carried out for the TGF to validate the temperatures calculated by the silica geothermometers. The block diagram that was acquired indicates that the geothermal field's reservoir temperatures range from 160 °C to 180 °C (Fig. 19).

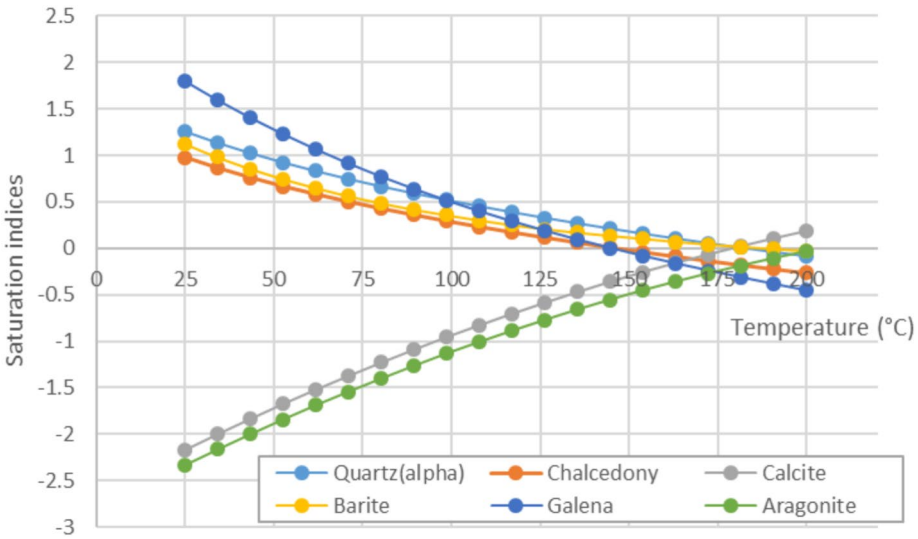

Fig. 18 Variation of the saturation indices of minerals according to temperature calculated with PhreeqC code. The convergence point corresponds to the equilibrium conditions of the geothermal fluid with minerals, i.e., the reservoir temperature

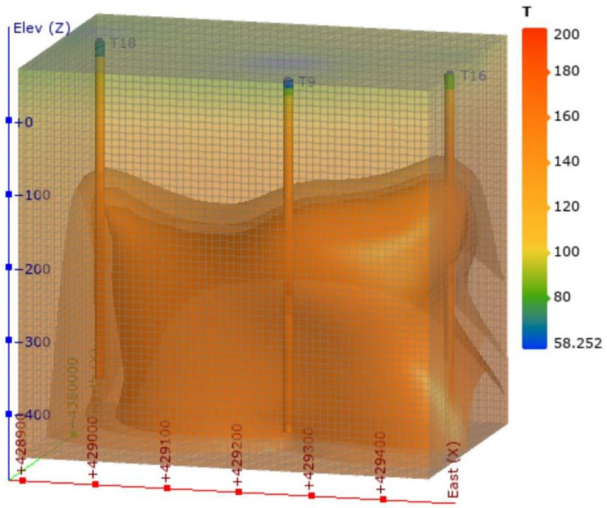

Fig. 19 Reservoir temperature modelling (3D thermal model was created in Leapfrog Geothermal software)

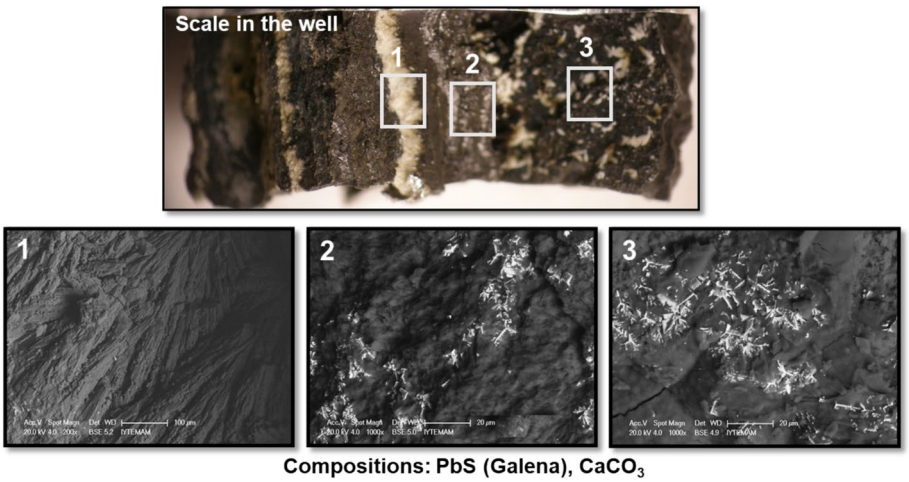

Fig. 20 SEM analysis of the scale sample collected from well T9

Evaluation/assessment of the scale samples

The scale samples were separated into two groups based on where they formed: in the surface pipeline (before the separator and vaporizer) and in the downhole (between 15 and 75 meters). The next sections provide an analysis of their morphology, elemental compositions, and structure.

The optical microscope image of the scale cross section in the well T9 is shown in Fig. 20. Structure is made up of layers that vary in thickness by millimeters. Because of the PbS and $CaCO_3$, respectively, the layers appear to be black and white, respectively

The dissolution of ferromagnesium crystals is responsible for the black color of scale with high concentrations of Mg, Pb, Fe, Si ions and traces of other element content. They are linked to volcanic rocks from the Miocene age that are composed of trachyte, andesite, and trachyte andesite. The TGF's reservoir rocks include these volcanic rocks,

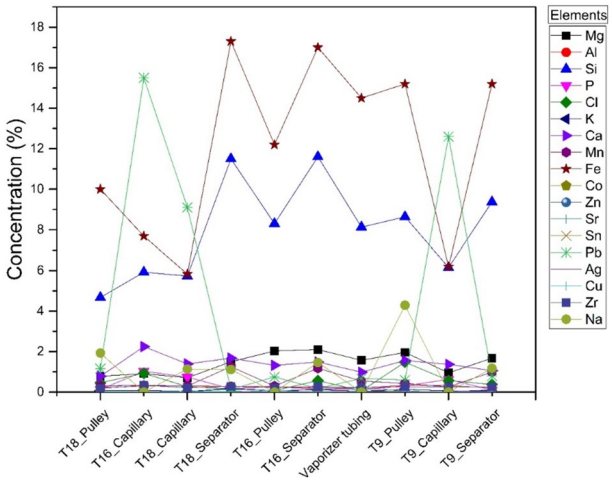

Fig. 21 Elemental compositions of the scale sample in the surface equipment system of the TGF

Table 6 Geometric dimensions of the geothermal well

Well interval	Length [m]	Cross-sectional diameter [m]
0 m–49 m	49	0.50
49 m–220 m	171	0.35
220 m–540 m	320	0.25

The feed zone of the well is located at 540 m and wellhead is at 0 m

which also include pyrite, hematite, quartz, K-feldspar, biotite, amphibole, sanidine, and chalcopyrite. According to Demir et al. (2014), the scale sample has a density of 2.18 to 2.88 g/cm^3. As shown in Fig. 20, PbS (galena) and $CaCO_3$ constitute the majority of the scale in the well T9. Using XRF, elemental analysis was performed on the scales that were collected from various parts of the TGF. The XRF data shows that the scale sample has elevated levels of Fe^{2+}, Pb^{2+}, Ca^{2+}, Na^{+}, Mg^{2+}, and Si^{4+} ions (Fig. 21).

The numerical analysis results

Determining the fluid composition in reservoir conditions is the first stage in the modeling process, highlighted in the numerical method. This is accomplished by first entering the fluid composition (see Table 2) into PhreeqC at laboratory conditions (pH = 5.6, Eh ≈ − 200 mV, Temp = 25 °C, P = 1 bar), and then raising the fluid's temperature and pressure to reservoir conditions (i.e., 160 °C and 50 bar). Because of the low charge balance (about − 0.6%), no adjustment of the chemical composition has been done. A final condition is then imposed on the fluid: the fluid is assumed to be in equilibrium with the rocks of the reservoir, in this case quartz and carbonates (more specifically calcite). The CO_2 partial pressure is changed in this case to 2.5 bar to meet the final requirement. Since fluids and carbonates in the formation rocks are typically believed to be in thermodynamic equilibrium, this constraint is reasonable. This limitation allows us to estimate the pH of

the fluid in the reservoir to be approximately 5.4, which is consistent with the degassing process taking place in the well but a little lower than the values measured at the surface.

The second stage is to evaluate the pressure and temperature profiles in the production well before assessing the downhole scaling risks. The GWELL code is utilized to input the T9 well's characteristic dimensions. Table 6 lists the measurements of the three segments that make up the total depth of 540 m (Baba et al. 2009). Each segment has a different cross section.

Downhole P and T profiles can be computed using the GWELL code in accordance with the well design and production rate. At the surface, the pressure decreases to roughly 3 bar from 50 bar in the reservoir (Fig. 22). Two tendencies are shown in Fig. 22, the first of which is the degassing-induced slope breakage at a depth of roughly 100 m. Degassing also has an impact on the temperature profile: a phase shift causes the temperature to abruptly drop at 100 m depth, reaching 140 °C near the surface (André et al. 2023).

The PhreeqC code is then used to simulate and assess the fluid's chemical reactivity in a one-dimensional column mimicking the well using the temperature and pressure profiles that were computed using the GWELL tool. Throughout its length (z=5 m), the borehole is discretized by 108 batch with their own P and T conditions. Every batch that has a liquid

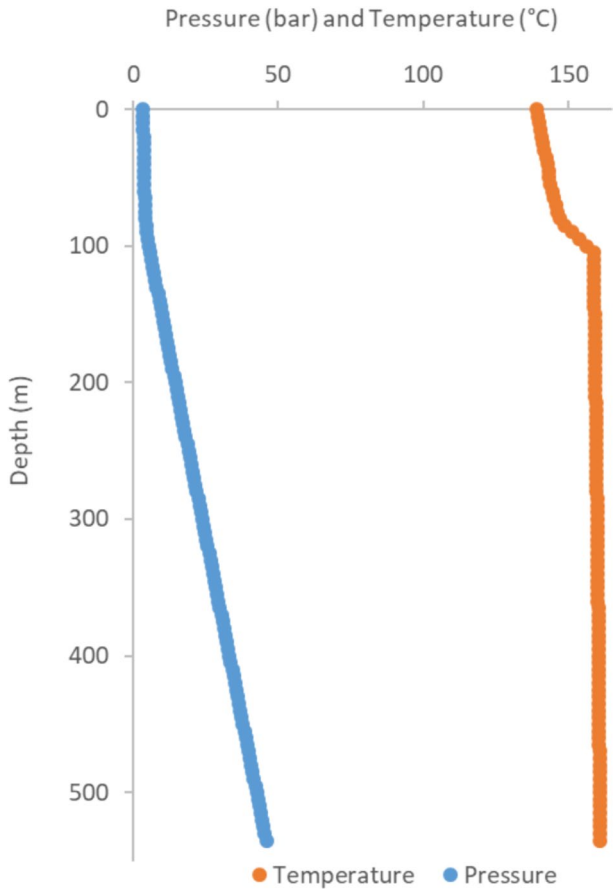

Fig. 22 Pressure (blue) and temperature (orange) profiles in the geothermal production well (André et al. 2023)

phase in it initially has a gas phase with a volume of zero. When the P and T parameters are favorable, this PhreeqC option permits the fluid to degas and the development of a gas phase. Calculations are done considering the gas phases in PhreeqC are always fully in equilibrium with the solution. Moreover, it is to note that PhreeqC does not allow the transport of gas between two adjacent cells. The previously determined chemical composition of the intake fluid is present.

The minerals that can precipitate during cooling can be determined by a first run conducted under batch settings without allowing for degassing.

The saturation index graphs (Fig. 23) demonstrate that the mineral wairakite in the geothermal wells is supersaturated at all temperatures. On the other hand, the mineral saponite ($Ca_{0.25}(Mg,Fe)_3((Si,Al)_4O_{10})(OH)_2–n(H_2O)$) is supersaturated in the geothermal waters over 75 °C. At all temperature ranges, the mineral sepiolite ($Mg_4Si_6O_{15}(OH)_2–6H_2O$) in Tuzla geothermal fluids is undersaturated. Sepiolite precipitation in the geothermal wells is, therefore, not a concern. Below 100 °C, amorphous silica and, more generally, silicate minerals (chalcedony, quartz) are saturated in geothermal fluids. The chemical reactivity in the well T9 is then the main topic of the simulation that follows.

A numerical run in the 1D column was conducted based on this observation in batch simulations. It makes it possible to calculate how the saturation indices of the primary minerals of interest change with depth. Within the well, precipitation of calcite ($CaCO_3$), quartz (SiO_2), galena (PbS), and barite ($BaSO_4$) is possible for the solution composition given (Fig. 24). As the fluid rises to the surface, these minerals' saturation indices do, in fact, increase along the production well.

As one approaches the wellhead, the calcite saturation index (continuous blue line in Fig. 24) rises. Initially close to equilibrium in the bottom section of the well, it turns positive at 100 m depth, suggesting that calcite is oversaturated and ready to precipitate within the well. The degassing is primarily responsible for this abrupt spike. Indeed, when $CO_{2(g)}$ exsolved according to Eq. 3, the system will tend to compensate this carbon loss using Eqs. 4 and 5. These two reactions consume protons and the consequence is a pH increase.

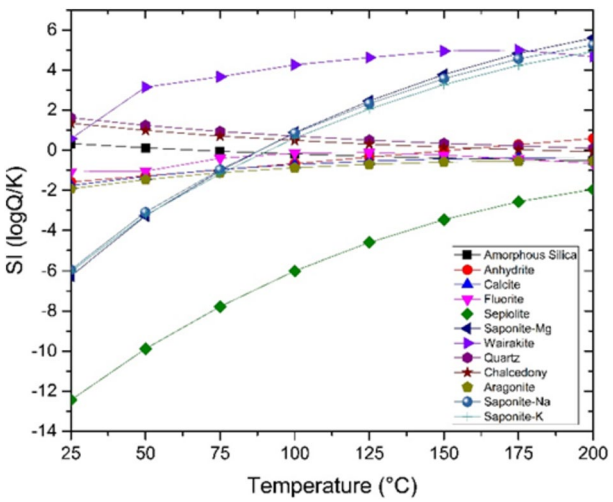

Fig. 23 Saturation indices for the well T9

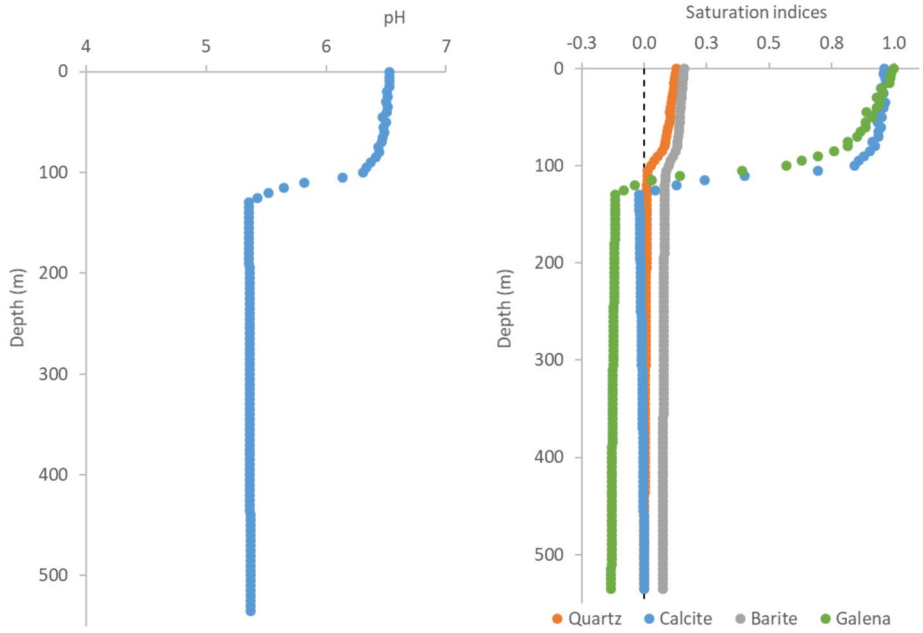

Fig. 24 Left: pH profile according to depth. Right: saturation index profile for minerals—calcite (blue), quartz (orange), galena (green) and barite (grey) in the geothermal production well. The dashed black line indicates equilibrium (saturation index of 0) for reference

Then, the carbon in solution becomes mainly under CO_3^{-2} form involving calcite oversaturation and the possibility of calcite precipitation according to Eq. 6:

$$CO_{2(aq)} = CO_{2(g)} \uparrow \tag{3}$$

$$CO_{2(aq)} + H_2O = HCO_3^- + H^+ \tag{4}$$

$$HCO_3^- = CO_3^{-2} + H^+ \tag{5}$$

$$CO_3^{-2} + Ca^{+2} = CaCO_3 \downarrow \tag{6}$$

On the other hand, quartz dissolves more readily at higher temperatures. As a result, the quartz saturation index (orange in Fig. 24) rises in the direction of the wellhead. Quartz has a near-zero saturation index near the feedzone. The quartz saturation index rises as one approaches the wellhead, suggesting that the mineral is oversaturated in the well and that precipitation may occur, mostly in the upper part of the well. Quartz and barite behave similarly in the simulation. Galena, a sulfide mineral, is initially undersaturated in the reservoir in comparison to the solution. It is still undersaturated below 100 m. Degassing, on the other hand, causes its saturation index to turn positive and increases the likelihood of precipitating such minerals. Indeed, the degassing of $H_2S_{(g)}$ involves the shift of the equilibrium (7) towards the formation of products. The consequence is that reactions 7–10 are impacted by these disequilibrium: protons are consumed, pH increases favouring the formation of S^{-2}:

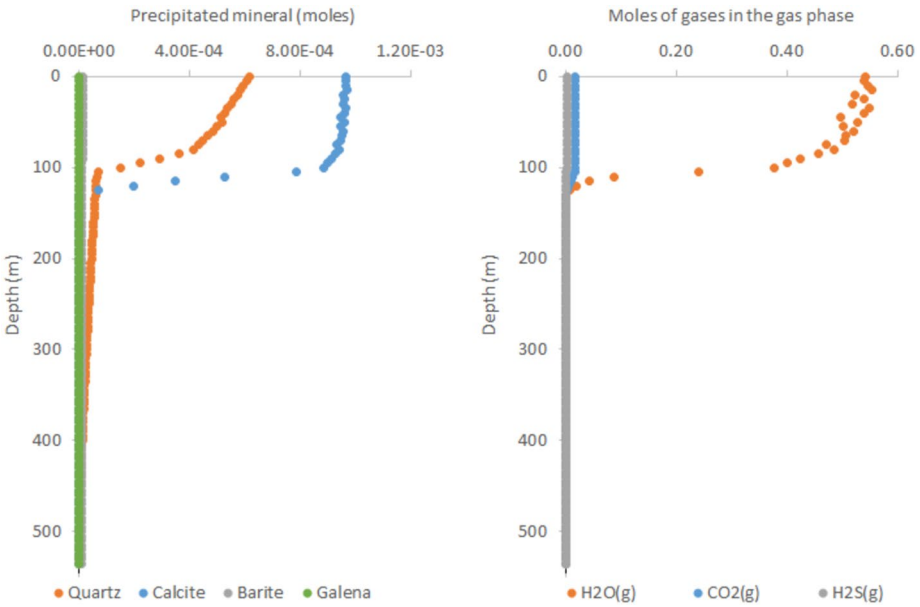

Fig. 25 Left: amount of precipitated minerals according to depth. Right: number of moles of gases in the gaseous phase in the geothermal production well (André et al. 2023)

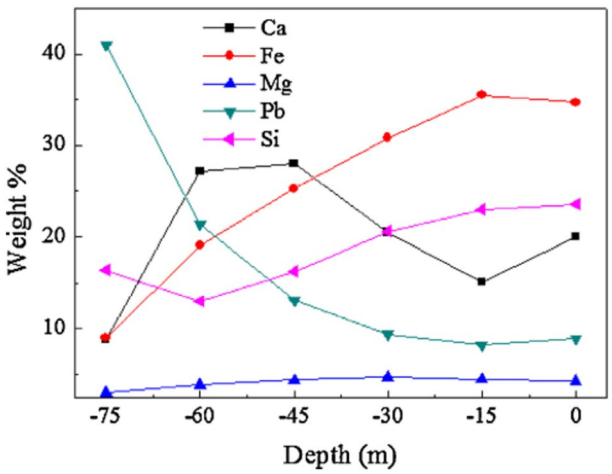

Fig. 26 Elemental composition of scales in the well obtained by XRF as a function of height the scale collected. The samples are collected from the surface of inhibitor hose (From Demir et al. 2014)

$$H_2S_{(aq)} = H_2S_{(g)} \uparrow \tag{7}$$

$$HS^- + H^+ = H_2S_{(aq)} \tag{8}$$

$$S^{-2} + H^+ = HS^- \tag{9}$$

$$S^{-2} + Pb^{+2} = PbS \downarrow \tag{10}$$

Then, the saturation index of galena becomes positive, and galena can potentially precipitate (Fig. 26).

The solution's thermodynamic equilibrium with regard to the four identified minerals is assumed in the final iteration. The amount of precipitated minerals is calculated by the code. Calculating the gas composition is also possible, assuming that it contains $CO_{2(g)}$, $H_2O_{(g)}$ and $H_2S_{(g)}$. Following the degassing, calcite precipitates, as shown in Fig. 25. Quartz precipitation is a result of the temperature dropping. Both galena and barite precipitate in very minute concentrations. Vapour makes up the majority of the gaseous phase, while tiny amounts of CO_2 and H_2S are also present (André et al. 2023).

Discussion

Regarding the lithology of the reservoir and the chemistry of the water, the TGF is among Türkiyey's most intricate geothermal fields. The most prevalent and challenging to deal with form of scaling in the Tuzla geothermal system is silicate-based scaling. Galena and $CaCO_3$ have been found in the borehole and surface pipeline, according to the elemental analysis of the scale samples. Sulfide scales, on the other hand, were exclusively discovered in downhole and not along the surface pipeline. Fe, Pb, Ca, Na, Mg, and Si elements are abundant in the scales. They are linked to volcanic rocks from the Miocene age that are composed of trachyte, andesite, and trachyte andesite. The TGF's reservoir rocks are these volcanic rocks, which include quartz, K-feldspar, biotite, amphibole, sanidine, chalcopyrite, pyrite, and hematite. The geothermal fluids exhibit supersaturation towards wairakite, undersaturation towards sepiolite, and supersaturation towards saponite beyond 75 °C. Sepiolite precipitation in the geothermal wells is, therefore, not a concern. The saturation indices of the geothermal fluids agree with the chemical species found in the scale that was collected from the pipeline; the principal constituents are NaCl and layered double hydroxide, which have amorphous forms resembling saponites.

A small quantity of precipitated minerals is anticipated before the degassing point, which is estimated to be about − 105 m, according to the numerical simulation, which also reveals that all of the mineral saturation indices stay near to 0. The model forecasts the deposition of mostly calcite with traces of galena, barite, and quartz. The degassing has a significant impact on the fluids' chemistry. Although the volume of minerals may be estimated using the model, the growth of the deposits' thickness cannot be predicted (the findings are not displayed here). However, the model does provide information on the scaling's composition.

These outcomes are compared with the site observations made by Demir et al. (2014). Demir et al. (2014) described the scaling composition in the TGF. Their research was concentrated on deposits that were found in the well between the surface and a depth of 75 m. Their elemental analysis indicates that Pb, Fe, Mg, Ca, and Si make up the majority of scale composition (Fig. 26). According to Fig. 26, these elements' concentrations vary with depth. Pb concentration drops with decreasing depth, whereas Fe concentration rises with decreasing depth. The author proved that, depending on depth, Ca^{2+} is mostly found in calcite and aragonite, while Pb is found in galena. They observed a rise in the

proportion of silica at the surface, which may be brought on by low temperatures. The numerical results are entirely compatible with all of these field observations.

As previously described, the actual approach is semi-quantitative. The next step could be to reach more quantitative results by adding:

- The kinetic rates of mineral precipitation. All calculations done here consider equilibrium state, i.e., an instantaneous equilibrium between the solution and the minerals. We know that many minerals are controlled by kinetic constraints that need to be included.
- The nucleation of the minerals and the potential transport of these minerals (as seeds) by the fluid. As for the previous remark, the equilibrium conditions suppose that the mineral precipitate in the well where their saturation indices become positive. We know that flow regimes in the well can modify this hypothesis.
- The deposition of the minerals on the well walls. Indeed, to be rigorous, we should include a deposition model to predict the evolution of the deposit thickness according to time.

At last, the modelling approach could be improved by better considering the gas phase in the modelling. In the present calculations, the gas phase is supposed immobile, i.e., it does not flow with the water towards the wellhead. This assumption affect the chemical composition of the aqueous phase in contact with the gas phase. The next step could be to use a fully coupled model, able to model multiphase systems.

Conclusions

The primary constituents in the deposit of Tuzla Geothermal Power Plant (GPP) are carbonate and metal silicate. Calcite and galena scaling are the main problems in the well, whilst Fe and Mg silicate are the main problems through the pipeline in the Tuzla GPP. The composition is rich in Fe and Mg silicates, depending on the system's location. This research discusses the effect of degassing on TGF scaling. The PhreeqC numerical model indicates that the degassing point is at about − 105 m. At this point, degassing significantly changes the fluid chemistry, and the model predicts the deposition of calcite along with smaller elements including galena, barite, and quartz. The model's output agrees with the experimental finding and field observations. The model provides significant insights into the composition of the scale. For example, depending on depth, the main sources of Ca and Pb are calcite and galena, respectively. Higher concentrations of silica are found close to the surface.

In addition to the analytical evaluation of geochemical data measured in geothermal resources, numerical models are extremely important. These methods will help to better understand the system and make predictions for the future. The results were clearly visible in the Tuzla geothermal field, which is geochemically very complex. The application of these methods in similar fields can highlight the problem of scaling in geothermal systems.

Acknowledgements

The authors are grateful to the two anonymous reviewers for their valuable contribution to improving our manuscript. We would like to thank the staff of Tuzla Geothermal Company., who supported the field work at every stage of the

project. The authors are also grateful to the Water Diplomacy Center (WDC) at Jordan University of Science and Technology (JUST) and the Swiss Agency for Development and Cooperation (SDC) for the fellowship.

Author contributions
Serhat Tonkul: Data collection, data evaluation, conceptual modeling, investigation Laurent André: Investigation, numerical modeling, editing Alper Baba: Methodology, data evaluation Mustafa M. Demir: Methodology Simona Regenspurg: Writing- reviewing and editing Katrin Kieling: Writing- reviewing and editing.

Funding
This study has received funding from the European Union's Horizon 2020 research and innovation programme under Grant agreement No 850626 (REFLECT). This study has also been funded by the European Union research and innovation programme under Grant agreement No 101058163 (CRM-geothermal).

Availability of data and materials
No datasets were generated or analysed during the current study.

Declarations

Ethics approval and consent to participate
Not applicable.

Competing interests
The authors declare no competing interests.

Received: 23 May 2024 Accepted: 22 October 2024
Published online: 15 January 2025

References

Akhmedov GY. Kinetics of growth of calcium carbonate deposits in geothermal systems. Therm Eng. 2009;56:909–13.
Alpin S. *Geothermal energy exploration in Turkey.* Paper presented at the Proceedings, Second United Nations Symposium on the Development and Use of Geothermal Resources; 1976.
Andhika M, Castaneda MCH, Regenspurg S. *Characterization of silica precipitation at geothermal conditions.* Paper presented at the World Geothermal Congress; 2015.
André L, Soulaine C, Shoeibi Omrani P. The H2020 REFLECT project: Deliverable 4.4–Numerical modelling of the geochemical behaviour of hot (type-A) and saline (type-C) fluids and validation against new data. 2023. https://doi.org/10.48440/gfz.4.8.2023.006
Arnórsson S. Deposition of calcium carbonate minerals from geothermal waters—theoretical considerations. Geothermics. 1989;18(1–2):33–9. https://doi.org/10.1016/0375-6505(89)90007-2.
Arnórsson S. Isotopic and chemical techniques in geothermal exploration, development and use. International Atomic Energy Agency. 2000;109–111.
Arnórsson S, Gunnlaugsson E, Svavarsson H. The chemistry of geothermal waters in Iceland. III. Chemical geothermometry in geothermal investigations. Geochim Cosmochim Acta. 1983;47(3):567–77.
Aunzo ZP, Bjornsson G, Bodvarsson GS. Wellbore Models GWELL, GWNACL, and HOLA. User's Guide. LBL-31428—UC 251; 1991.
Baba A, Yuce G, Deniz O, Ugurluoglu DY. Hydrochemical and isotopic composition of Tuzla geothermal field (Canakkale-Turkey) and its environmental impacts. Environ Forensics. 2009;10(2):144–61. https://doi.org/10.1080/15275920902873418.
Baba A, Demir MM, Koç GA, Tuğcu C. Hydrogeological properties of hyper-saline geothermal brine and application of inhibiting siliceous scale via pH modification. Geothermics. 2015;53:406–12. https://doi.org/10.1016/j.geothermics.2014.08.007.
Baba A, Tonkul S. The H2020 REFLECT project: Deliverable 1.2-Conceptual model for the Tuzla geothermal site. 2022. https://doi.org/10.48440/gfz.4.8.2022.006.
Barelli A, Corsi R, Del Pizzo G, Scali C. A two-phase flow model for geothermal wells in the presence of non-condensable gas. Geothermics. 1982;11(3):175–91.
Blanc P, Lassin A, Piantone P, Azaroual M, Jacquemet N, Fabbri A, Gaucher EC. Thermoddem: a geochemical database focused on low temperature water/rock interactions and waste materials. Appl Geochem. 2012;27:2107–16.
Brown K. Antimony and arsenic sulfide scaling in geothermal binary plants. Paper presented at the Proceedings International Workshop on Mineral Scaling. 2011.
Cao B, Ma Y, Liu M, Li S, Tian H, Feng G. Predictions of locations of flash point and calcite scaling of geothermal fluids in wellbore by chemical and thermodynamic simulations. Geothermics. 2024;121: 103057. https://doi.org/10.1016/j.geothermics.2024.103057.
Cerclet L, Courcelles B, Pasquier P. Reactive transport model predicting calcite precipitation: case of a dynamically operated standing column well. Geothermics. 2023;115: 102828. https://doi.org/10.1016/j.geothermics.2023.102828.
Craig H. Standard for reporting concentrations of deuterium and oxygen-18 in natural waters. Science. 1961;133(3467):1833–4.
Demir MM, Baba A, Atilla V, İnanlı M. Types of the scaling in hyper saline geothermal system in northwest Turkey. Geothermics. 2014;50:1–9. https://doi.org/10.1016/j.geothermics.2013.08.003.
Ellis A, Mahon W. Chemistry and Geothermal Systems Academic Press New York. 1977.

Ercan T, Türkecan A. Bati Anadolu-Ege adalari-Yunanistan ve Bulgaristan'daki plütonlarin gözden geçirilisi. Paper presented at the Ketin simpozyumu; 1985.
Fournier R. Chemical geothermometers and mixing models for geothermal systems. Geothermics. 1977;5(1–4):41–50. https://doi.org/10.1016/0375-6505(77)90007-4.
Fournier RO, Potter IR. Magnesium correction to the Na^+ K^+ Ca chemical geothermometer. Geochim Cosmochim Acta. 1979;43(9):1543–50. https://doi.org/10.1016/0016-7037(79)90147-9.
Fournier R, Potter I. Revised and expanded silica (quartz) geothermometer. Bull., Geotherm. Resour. Counc.(Davis, Calif.);(United States). 1982;11(10).
Fournier R, Truesdell A. An empirical Na^+ K^+ Ca geothermometer for natural waters. Geochim Cosmochim Acta. 1973;37(5):1255–75. https://doi.org/10.1016/0016-7037(73)90060-4.
Gallup DL. Aluminum silicate scale formation and inhibition: scale characterization and laboratory experiments. Geothermics. 1997;26(4):483–99. https://doi.org/10.1016/S0375-6505(97)00003-5.
Gallup DL. Investigations of organic inhibitors for silica scale control in geothermal brines. Geothermics. 2002;31(4):415–30. https://doi.org/10.1016/S0375-6505(02)00004-4.
Gallup DL, Barcelon E. Investigations of organic inhibitors for silica scale control from geothermal brines–II. Geothermics. 2005;34(6):756–71. https://doi.org/10.1016/j.geothermics.2005.09.002.
García AV, Thomsen K, Stenby EH. Prediction of mineral scale formation in geothermal and oilfield operations using the extended UNIQUAC model: part I. Sulfate scaling minerals. Geothermics. 2005;34(1):61–97. https://doi.org/10.1016/j.geothermics.2006.03.001.
Gat J, Carmi I. Evolution of the isotopic composition of atmospheric waters in the Mediterranean Sea area. J Geophys Res. 1970;75(15):3039–48.
Giggenbach WF. Geothermal solute equilibria. derivation of Na-K-Mg-Ca geoindicators. Geochim Cosmochim Acta. 1988;52(12):2749–65. https://doi.org/10.1016/0016-7037(88)90143-3.
Gunnarsson I, Arnórsson S. Impact of silica scaling on the efficiency of heat extraction from high-temperature geothermal fluids. Geothermics. 2005;34(3):320–9. https://doi.org/10.1016/j.geothermics.2005.02.002.
Gunnlaugsson E, Einarsson AR. Magnesium-silicate scaling in mixture of geothermal water and deaerated fresh water in a district heating system. Geothermics. 1989;18(1–2):113–20. https://doi.org/10.1016/0375-6505(89)90017-5.
Helgeson HC, Kirkham DH, Flowers GC. Theoretical prediction of the thermodynamic behavior of aqueous electrolytes by high pressures and temperatures; IV, calculation of activity coefficients, osmotic coefficients, and apparent molal and standard and relative partial molal properties to 600 °C. Am J Sci. 1981;281:1249–516. https://doi.org/10.2475/ajs.281.10.1249.
Honegger J, Czernichowski-Lauriol I, Criaud A, Menjoz A, Sainson S, Guezennec J. Detailed study of sulfide scaling at la courneuue nord, a geothermal exploitation of the Paris Basin. France Geothermics. 1989;18(1–2):137–44. https://doi.org/10.1016/0375-6505(89)90020-5.
Ichikuni M. Chemistry of silica scale formed from geothermal waters. Chikyukagaku Geochem. 1983;17:137–41.
Ikeda R, Ueda A. Experimental field investigations of inhibitors for controlling silica scale in geothermal brine at the Sumikawa geothermal plant, Akita Prefecture, Japan. Geothermics. 2017;70:305–13. https://doi.org/10.1016/j.geothermics.2017.06.017.
Juranek J, Škollová Z, Harnova J. "Minequa"—Part I. A program for computing the chemistry of calcium carbonate in mineralized and thermal waters. Geothermics. 1987;16(3):263–70. https://doi.org/10.1016/0375-6505(87)90005-8.
Karamanderesi IH. Hydrothermal alternation in well Tuzla T-2. Canakkale: United Nations University; 1986.
Kloppmann W, Négrel P, Casanova J, Klinge H, Schelkes K, Guerrot C. Halite dissolution derived brines in the vicinity of a Permian salt dome (N German Basin) Evidence from boron, strontium, oxygen, and hydrogen isotopes. Geochim Cosmochim Acta. 2001;65(22):4087–101. https://doi.org/10.1016/S0016-7037(01)00640-8.
Köhl B, Elsner M, Baumann T. Hydrochemical and operational parameters driving carbonate scale kinetics at geothermal facilities in the Bavarian Molasse Basin. Geothermal Energy. 2020;8(1):26. https://doi.org/10.1186/s40517-020-00180-x.
Kristmannsdóttir H. Types of scaling occurring by geothermal utilization in Iceland. Geothermics. 1989;18(1–2):183–90. https://doi.org/10.1016/0375-6505(89)90026-6.
Mundhenk N, Huttenloch P, Sanjuan B, Kohl T, Steger H, Zorn R. Corrosion and scaling as interrelated phenomena in an operating geothermal power plant. Corros Sci. 2013;70:17–28.
Mützenberg SR. Westliche Biga-Halbinsel (Canakkale, Türkei): Beziehung zwischen geologie, tektonik und entwicklung der thermalquellen. ETH Zurich; 1990.
Nieva D, Nieva R. Developments in geothermal energy in Mexico—part twelve. A cationic geothermometer for prospecting of geothermal resources. Heat Recovery Syst CHP. 1987;7(3):243–58.
Ölçenoğlu K. Scaling in the reservoir in Kizildere geothermal field. Turkey Geothermics. 1986;15(5–6):731–4. https://doi.org/10.1016/0375-6505(86)90085-4.
Pambudi NA, Itoi R, Yamashiro R, Alam BYCS, Tusara L, Jalilinasrabady S, Khasani J. The behavior of silica in geothermal brine from Dieng geothermal power plant, Indonesia. Geothermics. 2015;54:109–14. https://doi.org/10.1016/j.geothermics.2014.12.003.
Parkhurst DL, Appelo C. Description of input and examples for PHREEQC version 3—a computer program for speciation, batch-reaction, one-dimensional transport, and inverse geochemical calculations. US Geol Survey Tech Methods. 2013;6(A43):497.
Pátzay G, Kármán FH, Póta G. Preliminary investigations of scaling and corrosion in high enthalpy geothermal wells in Hungary. Geothermics. 2003;32(4–6):627–38. https://doi.org/10.1016/S0375-6505(03)00068-3.
Potapov V, Kashpura V, Alekseev V. A study of the growth of deposits in geothermal power systems. Therm Eng. 2001;48(5):395–400.
Ryley D. The mass discharge of a geofluid from a geothermal reservoir—well system with flashing flow in the bore. Geothermics. 1980;9(3–4):221–35. https://doi.org/10.1016/0375-6505(80)90001-2.
Samilgil E. Hydrogeological report of geothermal energy possibility survey of hot springs of Kestanbol and Tuzla village of Canakkale. MTA report. 1966;4274.

Satman A, Ugur Z, Onur M. The effect of calcite deposition on geothermal well inflow performance. Geothermics. 1999;28(3):425–44. https://doi.org/10.1016/S0375-6505(99)00016-4.
Şener M, Gevrek AI. Distribution and significance of hydrothermal alteration minerals in the Tuzla hydrothermal system, Canakkale, Turkey. J Volcanol Geoth Res. 2000;96(3–4):215–28. https://doi.org/10.1016/S0377-0273(99)00152-3.
Şimşek Ş, Yıldırım N, Gülgör A. Developmental and environmental effects of the Kızıldere geothermal power project, Turkey. Geothermics. 2005;34(2):234–51. https://doi.org/10.1016/j.geothermics.2004.12.005.
Tanger JC, Helgeson HC. Calculation of the thermodynamic and transport properties of aqueous species at high pressures and temperatures; revised equations of state for the standard partial molal properties of ions and electrolytes. Am J Sci. 1988;288:19–98. https://doi.org/10.2475/ajs.288.1.19.
Tobler DJ, Benning LG. In situ and time resolved nucleation and growth of silica nanoparticles forming under simulated geothermal conditions. Geochim Cosmochim Acta. 2013;114:156–68. https://doi.org/10.1016/j.gca.2013.03.045.
Tonani F. Some remarks on the application of geochemical techniques in geothermal exploration. Paper presented at the Advances in European Geothermal Research: Proceedings of the Second International Seminar on the Results of EC Geothermal Energy Research, held in Strasbourg; 1980.
Truesdell A. Summary of section III-geochemical techniques in exploration. Paper presented at the Proc. 2nd UN Symp. on the Development and Use of Geothermal Resources; 1976.
Tut Haklıdır FS, Balaban TÖ. A review of mineral precipitation and effective scale inhibition methods at geothermal power plants in West Anatolia (Turkey). Geothermics. 2019;80:103–18. https://doi.org/10.1016/j.geothermics.2019.02.013.
Tut Haklıdır FS, Şengün R, Aydın H. Characterization and Comparison of geothermal fluids geochemistry within the Kızıldere Geothermal Field in Turkey: new findings with power capacity expanding studies. Geothermics. 2021;94:102110. https://doi.org/10.1016/j.geothermics.2021.102110.
Urgun S. The geology of Tuzla–Kestanbol (Canakkale) surrounding and geothermal energy possibility. MTA report. 1971;4664.
Usda A, Kato H, Miyauchi T, Kato K. Investigation of pH control method to avoid silica scaling in the Sumikawa geothermal field. J Geothermal Res Soc Japan. 2003;25(3):163–77. https://doi.org/10.11367/grsj1979.25.163.
Utami P. Characteristics of the Kamojang geothermal reservoir (West Java) as revealed by its hydrothermal alteration mineralogy. Paper presented at the Proceedings world geothermal congress; 2000.
Yokoyama T, Ueda A, Kato K, Mogi K, Matsuo S. A study of the alumina–silica gel adsorbent for the removal of silicic acid from geothermal water: increase in adsorption capacity of the adsorbent due to formation of amorphous aluminosilicate by adsorption of silicic acid. J Colloid Interface Sci. 2002;252(1):1–5. https://doi.org/10.1006/jcis.2002.8382.

Publisher's Note